ASME Turbo Expo 2021: Turbomachinery Technical Conference and Exposition,
7-11 June 2021, Volume 5B, Paper: GT2021-59995
DOI:10.1115/GT2021-59995

PHYSICS-BASED THERMAL MANAGEMENT SYSTEM COMPONENTS DESIGN FOR ALL-ELECTRIC PROPULSION SYSTEMS

Soheil Jafari
Cranfield University
Bedfordshire, United Kingdom
S.Jafari@cranfield.ac.uk

Theoklis Nikolaidis
Cranfield University
Bedfordshire, United Kingdom
t.nikolaidis@cranfield.ac.uk

Roopesh Chowdary Sureddi
Cranfield University
Bedfordshire, United Kingdom
s.roopesh03@gmail.com

ABSTRACT

Although electrification allows a significant reduction in fuel burn, noise, and emissions, one of the main challenges in this technology is to deal with the thermal loads generated by the electrified propulsion system components. This is to guarantee the safe and optimal operation of the propulsion system as well as the aircraft. This challenge needs to be addressed to enable this important technology to be adopted by aircraft manufacturers. This paper presents a methodological approach to calculate the heat load values generated by electric components in All-Electric Propulsion (AEP) architectures. Initially, the architecture of an AEP system will be presented and explained. Then, for each component, physics-based models based on associated heat loss mechanisms will be developed and presented. For this purpose, thermal models for battery packs, electric motors, inverters, and rectifiers are generated and a MATLAB/Simulink library is developed to calculate the thermal loads generated by each component at different working conditions. The developed models' results are validated against publicly available data to confirm the effectiveness of the proposed approach. The simulation results confirm that the developed library is able to predict the thermal loads generated by lithium-ion battery packs, permanent magnet synchronous electric motors, multi-stage inverters, and rectifiers with less than 1%, 9.9%, 9.2%, and 0.5% errors respectively. Finally, an AEP architecture is simulated as the case study and the total heat loads generated by different components have been calculated at the design point to confirm the capability of the developed framework in system-level analyses.

Keywords: Thermal Management System, All Electric Propulsion, Heat Loss Calculation, Physics-based Models, MATLAB Toolbox

1. INTRODUCTION

Waves of electrification in the aerospace sector have proposed radical concepts and structures for both aircraft and green propulsion systems. These embodiments are presented for different classes from delivery drones to large commercial aircraft. The way that the thermal loads are managed in electrified propulsion systems is still a practical challenge in the roadmap of the electrification of propulsion systems. This challenge needs to be addressed to enable this important technology to be adopted by aircraft manufacturers. As electrical components are more sensitive to overheating, having a practical tool for precise prediction of the generated thermal loads in electrified propulsion systems is becoming a necessity, even in the first steps of the conceptual design procedure, to maintain the expected efficiency and life span of the components. Although there are several published studies on the methods and approaches for calculation of excess heat loads generated in battery packs [1][2][3], electrical machines [4][5][6][7], and power converters [8][9], the lack of a system-level approach for developing a modular library able to predict the total heat load in All-Electric Propulsion (AEP) system architectures, is the main motivation of doing this piece of research.

This paper presents the procedure of developing a MATLAB library for the calculation of heat loads in AEP system components and the whole architecture. The study of battery packs is focused on lithium-ion type with both series and parallel cells. The effects of ambient temperature on the generated heat loads in battery packs are also taken into account. The Permanent Magnet Synchronous Motor (PMSM) type is selected for electric motor modelling where motor core losses, magnet losses, and copper losses are considered and simulated. Conduction and switching losses are modelled in the modern state of the art multi-stage inverters and rectifiers. All developed modules are validated against publicly available data to confirm the validity of the proposed approach. Moreover, in order to confirm the capability of the developed toolbox for system-level applications, an AEP architecture is simulated as the case study and the total heat loads generated by different components have been calculated at the design point. The contribution of each component in the total heat load could also be shown with the toolbox to enable the designer to find the main source of the heat in AEP for special attention.

2. MODELLING OF BATTERY PACK

Battery packs are the main power source of electricity in an AEP system. With modern technology development, there are a large number of choices in rechargeable batteries available for use in electric vehicles like nickel-cadmium, lithium-ion, nickel-metal hydride, lithium-ion polymer, lead-acid, and many other compositions [10]. According to the literature, lithium-ion batteries are the most promising candidate for aerospace applications with the highest specific energy compared to others.

Lithium-ion batteries are in the form of cells combined in series and/or parallel connections to provide the required output voltage forming the battery packs [11]. The amount of heat loss in lithium-ion battery packs depends on the equivalent resistance, current, and the number of cells of the whole pack as follow:

$$P = R_{eq} * I^2 * N \quad (1)$$

Where "P" is the total heat load in KW, "R_{eq}" is the equivalence internal resistance in Ω, "I" is the current in A, and "N" is the number of the cells. "R_{eq}" changes with the way of how the cells are connected. If the cells are connected in series, then:

$$R_{eq} = R_1 + R_2 + R_3 + \cdots + R_n \quad (2)$$

And if the cells are connected in parallel, then:

$$\frac{1}{R_{eq}} = \frac{1}{R_1} + \frac{1}{R_2} + \frac{1}{R_3} + \cdots + \frac{1}{R_n} \quad (3)$$

R_1, R_2, R_3, …, R_n are the individual resistances of each cell connected in series or parallel.

The resistance of lithium-ion batteries is affected by the operating temperature and the State of Charge (SOC) of the batteries. The effects are discussed in detail in [10] and [12]. For example, a theoretical relationship for a 18650B lithium-ion battery states that with the rise of temperature by each degree there is a drop of the output voltage by 0.055%, and this number changes for different lithium-ion batteries. This drop of final required output leads to the incorporation of a higher number of cells to compensate for the loss which in turn leads to the rise of temperature [13]. The internal resistance of a cell mainly depends on the life of a cell. For a newly opened cell, its internal resistance can be measured at 0.01Ω but for a used and worn-out cell it is measured at 0.04 – 0.05 Ω. As this study aims to develop a Battery pack model for aerospace applications, the effect of ambient temperature should also be modelled to enable designers and researchers to calculate the heat loss values at different flight phases. So, the discharge of current for a cell is modelled as a function of the temperature as indicated in Table 1 [14].

TABLE 1: TEMPERATURE DEPENDENCY OF CURRENT DISCHARGE CAPACITY

Discharge Temperature	-20°C	-10°C	0°C	25°C	60°C
Current discharge capacity	60%	75%	80%	100%	95%

Figure 1 shows the in-house MATLAB App developed for the calculation of total heat loss for a Lithium-ion battery pack in the Centre for propulsion engineering at Cranfield University.

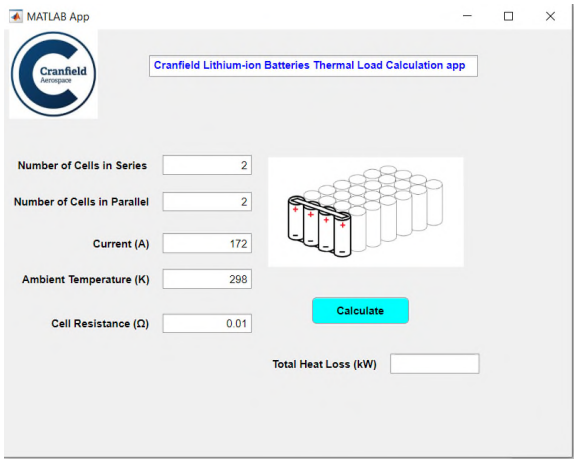

FIGURE 1: HEAT LOAD CALCULATION APP FOR LITHIUM-ION BATTERIES WITH AMBIENT TEMPERATURE CONSIDERATION

In order to confirm the validity of the developed model, the results obtained for the Li-Ion battery presented in [15] are reproduced here. The characteristics of the case study are shown in Table 2. For the calculation of the thermal load in [15], the battery module is assumed to be new and the internal resistance is considered as 0.01Ω. Moreover, the model presented in [15] has not the capability of changing the ambient temperature. So, the temperature is set to 25°C to replicate the results. The outcome of the developed app is 295.8 W/cell which is exactly the same as the value reported in [15]. It is worth mentioning that the effect of degradation in the battery pack is huge. For reference purposes, for the same model of the battery pack, the total heat load at 0.05Ω would be 5917 W.

TABLE 2: PROPERTIES OF THE BATTERY MODULE

Module Voltage	7.5 V
Module Current	172 A
Cell capacity	86 Ah
Number of Cells	4 (2 series + 2 parallel)
Temperature	25°C
Weight	4.8 Kg Approximate

3. MODELLING OF ELECTRIC MOTORS

In the AEP system, an electric motor is to convert the electrical energy from the power source into mechanical energy providing the required propulsive force. There are mainly two types of electric motors, Permanent Magnet Synchronous Motor (PMSM) and induction motor. But compared to induction motors, PMSMs have higher power density and efficiency [4][16]. So, PMSMs are extensively used and for this reason, PMSM is considered for the calculation of heat losses in this study.

There are three main losses in a PMSM:

- Motor Core losses
- Magnetic losses

- Copper losses

3.1 Motor Core Losses

Motor core losses are caused by the rotor core of the motor and can be calculated from the equation developed by Steinmetz as follow [5]:

$$P_{core} = K_h f^2 B_m^2 + K_e f^2 B_m^2 + K_a f^{1.5} B_m^{1.5} \quad (4)$$

Where K_h, K_e, and K_a are the coefficients of hysteresis loss, eddy current loss, and additional losses respectively. "f" is the frequency in Hz, and "B_m" is the magnetic flux density amplitude in T.

3.2 Magnetic Losses

Magnetic losses in the motor are due to the permanent magnet in the motor. These magnetic losses can be calculated from the equation developed from the eddy current model and the total magnetic losses are given by equation 5 [7]:

$$P_{mag} = \rho_m J_m^2 = \frac{W^2 \pi^2 f^2}{4\rho_m} \sum_{n=1}^{\infty} \frac{n^2 C_n^2}{2} \quad (5)$$

Where "ρ_m" is the electrical resistivity of the magnet in μΩ·m, "J_m" is the eddy current density of the magnet in W, "W" is the width of the magnet in m, "C_n" is the coefficient of friction and "f" is the frequency of the motor in Hz.

3.3 Copper Losses

Copper losses in the motor are caused by the stator and windings of the stator in the motor. Copper losses in the motor can be determined by equation 6 [7]:

$$P_{copper} = \rho_{copper} l_w \iint_s^{\cdot} (J_s + J_e)^2 ds \quad (6)$$

$$\rho_{copper} = \rho_0 (1 + \alpha (T - T_0)) \quad (7)$$

Where "ρ_{copper}" and "ρ_0" are the copper resistivity at temperature T and T_0 respectively, "J_s" is current source density in winding, "J_e" is eddy current density in winding, "l_w" is the active length of winging in m and "α" is the temperature coefficient of copper resistivity.

Figure 2 shows the in-house app developed for the calculation of total heat loss for a PMSM in the Centre for propulsion engineering at Cranfield University.

The inputs of the model are the frequency of the motor in Hz, Copper Winding Length in m, and Electric Resistivity. The frequency of the motor can be obtained from the datasheet of the selected motor. Winding length can be calculated from the outer diameter, inner diameter, and length of the rotor which is also available in the datasheet. Electric resistivity can be calculated using the rpm and torque at which the heat load is to be calculated. Figures for the selection of the values of coefficients of hysteresis loss and eddy current loss as a function of magnetic flux density, B_m, are presented in detail in [17].

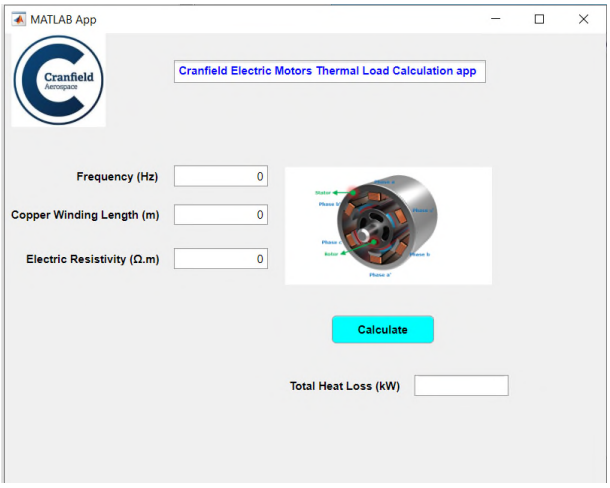

FIGURE 2: HEAT LOAD CALCULATION APP FOR ELECTRIC MOTOR

For validation of the developed model, results from [6] for an electric motor at 3000 rpm and 70 Nm torque and results from [18] for an electric motor at 6000 rpm and 47.5 Nm torque are used. Table 3 shows the generalized values of few parameters required in the calculation of heat load commonly used and widely recognized. Tables 4 and 5 show the parameters of the first and the second electric motors used for validation of simulated results respectively.

TABLE 3: CASE STUDIES INPUTS

Magnetic Flux Density	1.9 T
Copper Resistivity	1.72 x 10-8 Ω.m

TABLE 4: PARAMETERS FOR ELETRIC MOTOR AT 3000 RPM AND 70 NM

Continuous Power	22 KW
Frequency	400 Hz
Diameter difference of rotor	80 mm
Length of rotor	120 mm

TABLE 5: PARAMETERS FOR ELETRIC MOTOR AT 6000 RPM AND 47.5 NM

Frequency	100 Hz
Base Speed	6000 rpm
Diameter difference of rotor	67 mm
Length of rotor	90 mm

Table 6 shows the compared results between Heat load obtained from the developed model and Electric Motor 1 and Electric Motor 2. It is observed that a maximum difference of 9.9% between the developed model and electric motor 1; And a difference of 1.5% between the developed model and the Electric motor 2.

TABLE 6: ELECTRIC MOTOR HEAT LOAD CALCULATION RESULTS

	Total Heat Load (published) (W)	Total Heat Load – (developed app)(W)
Electric Motor 1 [6]	539.4	592.7
Electric Motor 2 [18]	1397	1418

4. MODELLING OF POWER CONVERTERS

Power converters are mainly classified based on the way in which they convert between Alternating Current (AC) and Direct Current (DC) as input or output [19]. Battery packs store the electricity in the form of DC power, but the motor and the power source from which batteries in the pack are recharged is in the form of AC power. This requires the AEP system to incorporate power converters. The battery management system in the AEP system which controls the recharge of the batteries has a rectifier that converts the AC power source to DC power for the batteries to be recharged. The Electronic Speed Controller consists of an inverter that converts the DC power from battery packs into AC power for the motor.

Losses in all the power converters are due to the Insulated-Gate Bipolar Transistor (IGBT) losses or diode losses. These losses are mainly due to the conduction losses and switching losses [20] [9] and are represented by subscripts "cond" and "SW" respectively.

$$P_{total} = P_{cond} + P_{SW} \quad (8)$$

The conduction and switching losses in inverters and rectifiers could be calculated as follows:

4.1 Inverters

The conduction losses in the inverter can be calculated by the following equations [21]:

$$P_{cond} = V_{CE(on)} * I_{C(on)} * D_{cond} \quad (9)$$

$$D_{cond} = \frac{t_{Level-i}}{T} \quad (10)$$

$$t_{Level-i} = 2(S_i(t_i - t_{i-1}) + (1 - S_{i+1})(t_{i+1} - 1) \quad (11)$$

$$t_i = \frac{\theta_i * T}{2\pi} \quad (12)$$

$$\theta_i = arcsin\frac{i}{A_r} \quad (13)$$

$$A_r = M * a \quad (14)$$

Where "V_{CE}" is the voltage in V, "I_C" is the current in A, "D_{cond}" is the correction coefficient for conduction losses, "t" is the time taken in a specific stage and the subscript indicates the stage in ns, "S" is the sinusoidal estimation for the specific stage, "θ_i" is the angle from the sinusoidal estimate of i^{th} stage, "M" is the modulation index, "a" is the number of voltage sources, "A_r" is the amplitude of the sinusoidal wave in m, "T" is the total period and "P_{cond}" is the total conduction losses. The subscripts "on" and "off" refers to the "on" and "off" state of the inverter.

The switching losses in the inverter can be calculated by the following equations [21]:

$$P_{SW} = F_{SW} * \left(E_{SW(on)} + E_{SW(off)}\right) * D_{SW} \quad (15)$$

$$E_{SW(on)} = \int_{t_0}^{t_4} V_{CE}(t) * I_C(t) \quad (16)$$

$$E_{SW(off)} = \int_{t_0}^{t_2} V_{CE}(t) * I_C(t) \quad (17)$$

$$D_{SW} = \frac{t_{SW}}{T} \quad (18)$$

$$t_{SW} = 2(\frac{T}{4} - t_1) \quad (19)$$

Where "P_{SW}" is the total switching losses in W, "t_{SW}" is the total time of switching in ns, "V_{CE}" is the voltage in V, "I_C" is the current A, "t" is the time taken for switching between stages in ns, "D_{SW}" is the correction coefficient for switching losses.

Figure 3 shows the MATLAB-Simulink model developed for the calculation of total heat load for a Multi-stage inverter based on the above equations. The inputs for the model are Voltage of the IGBT in the inverter as input 1 (Voltage) in V, Current in A, Number of Stages, Frequency in Hz, and Power Factor. All Five inputs can be obtained from the datasheet of any selected inverter. A modern state of the art multi-stage inverter is considered to be a 5-stage inverter. So, the MATLAB-Simulink model is developed for the inverters with stages from 1 to 5.

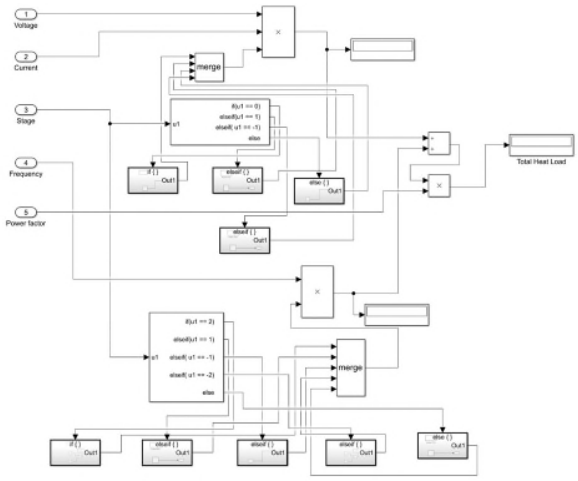

FIGURE 3: INVERTER HEAT LOSS CALCULATION MODEL

Moreover, tables 7 and 8 show the correction coefficients for conduction and switching losses required for equations 9 and 15 respectively.

TABLE 7: CORRECTION COEFFICIENTS FOR CONDUCTION LOSS

Stage	1	2	3	4	5
Correction Coefficient	0.218	0.201	0.162	0.201	0.218

TABLE 8: CORRECTION COEFFICIENTS FOR SWITCHING LOSS

Stage	1-2	2-3	3-4	4-5
Correction Coefficient	0.334	0.165	0.165	0.334

For validation purposes of the developed model, the models presented in [22] are used. The selected inverter is SEMIX151GD066HD (dual IGBT) and the properties of the inverter obtained from [22] are given in Table 8. The results from the developed model are compared with different results taken from [22] (PSIM inverter model and Semisel program) and are shown in Table 9 (the results for the PSIM model are from the numerical method and Semisel is an open-source program which can predict the heat load depending on the circuit of the inverter). The total heat load shows that the developed model differs at a maximum of 9.2% in comparison with Semisel and a 2.9% difference when compared to results from PSIM.

TABLE 9: VALIDATION OF THE INVERTER MODEL

	Total Heat Load (W)
PSIM	1070.1
Semisel	1008
Results from the developed model	1101.03

4.2 Rectifiers

Losses in the rectifiers can be calculated by equation 20 [8] [23]:

$$P_{total} = \frac{V_{FM} I_{FM} t_{on}}{T} + \frac{V_R I_R t_{off}}{T} + \frac{0.5 Q_{rr} V_R}{T} + \frac{0.318 V_{frM} I_{FM} t_{fr}}{T} \quad (20)$$

Where "V_{FM}" is the maximum forward voltage in V. "I_{FM}" is the maximum forward current in A, "t_{on}" is the total time for rectifier in switched on stage, "t_{off}" is the total time for rectifier in switched-off state in ns, "T" is the total time, "V_R" is the reverse voltage in V, "I_R" is the reverse current in A, "V_{frM}" is the maximum forward recovery voltage in V and "Q_{rr}" is the reverse recovery charge of the rectifier in µC. Both the conduction losses and the switching losses are combined and formed equation 20.

Figure 4 shows an in-house app developed for the calculation of total heat loss for rectifiers in the Centre for propulsion engineering at Cranfield University. The inputs of the model are the Forward voltage in V, Reverse voltage in V, T_{on} in ns, T_{off} in ns, Total time in ns, Reverse recovery charge in µC, and Current in A. T_{on} and T_{off} are the time of rise and time of fall for the rectifier between the states of switching on and off respectively. The total time is the time taken by the rectifier for switching for the total time of operation. Forward and reverse voltages are the input and output voltages respectively. As Total time depends on the time of operation, it could be obtained by a simple calculation from the total time of operation and the switching time given in the datasheet. All the other six inputs can obtain directly from the datasheet.

For the validation of the developed model, an experiment conducted on a rectifier CREE C2M0025120D is taken into consideration [24]. The parameters of the rectifier are listed in table 10. Table 11 compares the result of the selected rectifier model and the simulated result from the developed model. A 0.4% difference between the results from the developed rectifier model and the selected rectifier is observed.

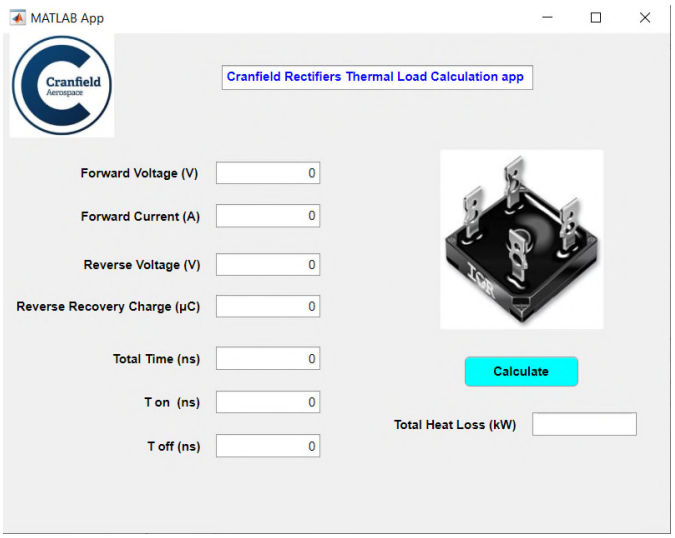

FIGURE 4: HEAT LOAD CALCULATION APP FOR RECTIFIERS

TABLE 10: PROPERTIES OF THE SELECTED RECTIFIER

Input Voltage	360-440 V_{ac}
Output Voltage	700 V_{dc}
Output Power	5 KW
Current	11.7 A
Frequency	50 KHz
T_{on}	52 ns
T_{off}	46 ns
Total time	72000 ns
Q_{rr}	284 µC

TABLE 11: VALIDATION OF THE RECTIFIER MODEL

CREE C2M0025120D	Total Heat Load (W)
Results from [24]	36.2
Results from the developed app	36.34

5. SYSTEM LEVEL MODEL

The developed MATLAB/Simulink modules are added together to form a library in MATLAB that could be used to simulate

different architectures for AEPs. The advantage of this library is its modular feature able to calculate heat loads in different sizes of electric systems at different working conditions.
As a case study, the architecture shown in figure 5 is simulated in this section. As Rectifier converts AC power to DC power and should be connected to the Battery Pack; and the ground power source will be connected to Rectifier. Inverters convert DC power to AC power, so the Inverter should be connected between Battery Pack and Electric Motor. So, in terms of power flow, the power from the ground source flows to the battery pack where it is stored through a rectifier. Then the stored power from the battery pack flows through an inverter and reaches the Electric Motor where this electrical power is converted to mechanical power. Which is in turn transferred to the propeller/fans depending on the electric motor. In recent years, there is a new device that's been developed that can act both as Rectifier and Inverter. It's a bi-directional device that can convert AC to DC when the flow is in one direction and when the flow is reversed it converts DC to AC. Figure 6 shows the MATLAB-Simulink developed model for the total heat load calculation of an AEP System.

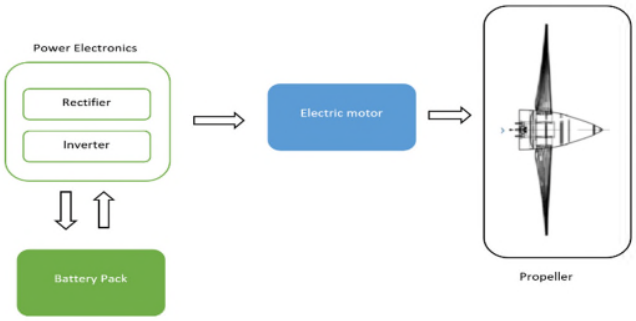

FIGURE 5: SIMULATED AEP ARCHITECTURE

For the case study of the AEP System, the components are selected to have the potential of making an AEP system for a 10-13 passenger aircraft. A PMSM with 750HP of power is selected, the battery pack configuration inspired by those of NASA X-57 Maxwell. Depending on the battery pack and motor specifications a suitable inverter and rectifier are chosen. The battery pack is divided into 16 modules, and each module is divided into 16 more sub-modules. Each sub-module has 20 Li-Ion cells connected in a 1S20P configuration, which means that all the 20 Li-Ion cells in the sub-module are connected in parallel. These sub-modules are then connected in the configuration of 16S1P in each module, which means there are 16 sub-modules that are connected in series. Then all the modules are connected in 16S2P configuration i.e. there are 2 modules that are connected in parallel and has 16 sub-modules connected in series, to form a whole Battery Pack. The specifications of the battery pack are given in table 12. This configuration is similar to that of the battery pack used in NASA X-57 Maxwell [3] with a slight change so the output voltage will be suitable for the selected motor, i.e. the change is that the X-57 Maxwell had only 8 sub-modules connected in series in each module but this battery pack will have 16 sub-modules.

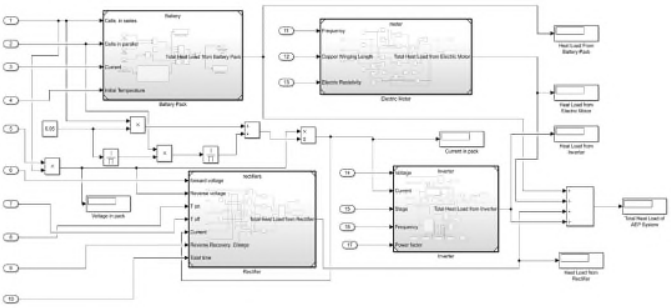

FIGURE 6: SIMULATION MODEL FOR AEP ARCHITECTURE

TABLE 12: SPECIFICATION OF THE BATTERY PACK

Total nominal Voltage	660 V
Current from each cell	9 A
Weight of each cell	48 grams
Sub-module configuration	1Sx20P
Module configuration	16Sx1P
Pack configuration	16Sx2P
Assumed initial temperature	15℃

The selected Electric motor is a motor that can produce 750 HP with a maximum power of 560 KW. It can be used in a single propeller aircraft with a capacity of 10-13 passengers like Cessna Caravan as the main engine or can be used in a large aircraft as a supporting source of power. The core rotor diameter and the length are not given out by the manufacturer, so these values are assumed from the data available on the outer dimensions of the motor and the previously made motors which were of lower power [25]. The specifications of the selected motor are given in table 13.
A suitable multi-stage inverter that can continuously provide the required voltage available from the battery pack to the electric motor is selected. The selected inverter is from Infineon company and the model was named FF600R06ME3, which was previously used in a two-seater aircraft mentioned in [20]. The specifications of the inverter are given in table 14.

TABLE 13: SPECIFICATION OF THE ELECTRIC MOTOR

Continuous Power	560 KW / 750 HP
Voltage	540 V
Diameter difference of rotor	624 mm
Length of rotor	450 mm
Efficiency	>93%
Base Speed	1900 RPM

TABLE 14: SPECIFICATION OF THE INVERTER

IGBT Voltage	4.2 V
Current	119 A
Frequency	800 Hz
Number of Stages	5
Power Factor	0.97

For a rectifier, a high current transformer rectifier unit is selected, the selected rectifier belongs to the VS-150 series developed by Vishay Semiconductors. It is generally used to convert the ground power given to an aircraft to start an Auxiliary Power Unit (APU) converting the AC ground power into DC power required by APU. In this case, it converts the AC ground power to DC to be stored in the battery pack. The specifications of the converter are given in table 15.

TABLE 15: SPECIFICATION OF THE RECTIFIER

Input Voltage	230-440 V_{ac}
Output Voltage	900 V_{dc}
Current	119 A
Frequency	400 Hz
T_{on}	26 ns
T_{off}	34 ns
Total time	47200 ns
Q_{rr}	319 µC

Results obtained from the selected components for the case study of the AEP System are given in table 16. The conditions taken for the case study is a cold day with 15°C of initial temperature at the flight condition of the take-off stage at which the maximum power is used by the system. It can be observed that the total heat load is calculated as 50.6 KW. The total power at take-off is at a maximum of 560 KW. So, the total heat loads are 9% of the total power. These results can be taken as an estimated value for the preliminary design of the thermal management system accordingly.

Figure 7 shows the contribution of each component in the total heat loss generated in the system. It can be observed that 75% of the total heat load is being produced from the battery packs, 23% from Electric Motor, 1% from Inverter, and 0.2% from rectifiers. As the largest amount of heat load is being released from the battery packs, the designed Thermal Management System should be able to efficiently utilize the cooling mechanism and/or heat exchangers to manage this amount of heat optimally. The advancement in the batteries technologies in the future can also significantly reduce the total amount of heat load for the AEP system.

TABLE 16: AEP ARCHITECTURE CASE STUDY RESULTS

	Heat Load (KW)
Battery Pack	38.15
Electric Motor	11.87
Inverter	0.46
Rectifier	0.10
Total AEP System	50.6

Although more tests and explorations are required to increase the accuracy and reliability of the developed toolbox, the current library could be considered as the first step in the design and development procedure of the thermal management systems for AEPs. The modular feature presented in this study can be used with any AEP system with just a slight adjustment in the components' inputs and boundary conditions.

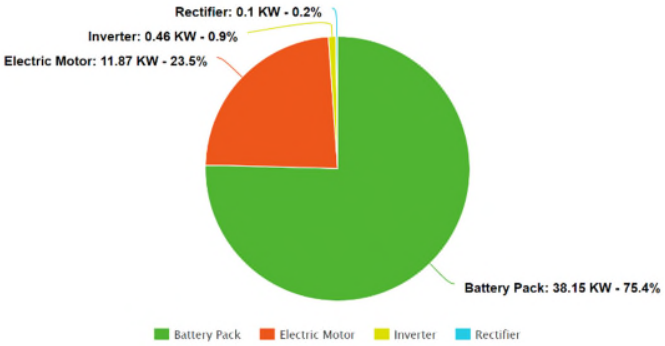

FIGURE 7: SIMULATION RESULTS FOR AEP ARCHITECTURE

6. CONCLUSION

A modular toolbox to calculate thermal heat loads in all-electric propulsion systems has been developed and validated in this study.

- The battery pack module is able to calculate heat loads in Lithium-ion battery packs with series and/or parallel cells connected with consideration of the ambient temperature effects.
- The electric motor module calculates different heat loss mechanisms in PMSM including motor core loss, magnetic loss, and copper loss.
- The inverter module calculates the conduction and switching losses in a modern state of the art multi-stage inverter.
- The rectifier loss can calculate conduction and switching losses in rectifiers with the capability of considering the time of rise and time of fall for the rectifier between the states of switching on and off respectively.

The simulation results confirm that the developed library is able to predict the thermal loads generated by the battery pack, electric motor, inverters, and rectifiers with less than 1%, 9.9%, 9.2%, and 0.5% errors respectively. Moreover, an AEP

architecture is simulated as the case study and the total heat loads generated by different components have been calculated at the design point. The total power at take-off is at a maximum of 560 KW and the tool obtains a heat load of 50.6 KW, which is 9% of the total power. The contribution of each component in this heat load also shows that the main source of heat in AEP is the battery. Therefore, special attention should be paid to the design and development of an optimized thermal management system for the battery in AEPs.

REFERENCES

[1] S. Madani, E. Schaltz, and S. Knudsen Kær, "Heat Loss Measurement of Lithium Titanate Oxide Batteries under Fast Charging Conditions by Employing Isothermal Calorimeter," *Batteries*, vol. 4, no. 4, p. 59, Nov. 2018.

[2] J. Zhang, L. Su, Z. Li, Y. Sun, and N. Wu, "The Evolution of Lithium-Ion Cell Thermal Safety with Aging Examined in a Battery Testing Calorimeter," *Batteries*, vol. 2, no. 2, p. 12, Apr. 2016.

[3] J. C. Chin, S. L. Schnulo, T. B. Miller, K. Prokopius, and J. Gray, "Battery performance modeling on maxwell x-57," *AIAA Scitech 2019 Forum*, no. January, 2019.

[4] A. Kumar, "Electric motor internal heat convection modelling and analysis," Chalmers University of Technology, 2018.

[5] J. C. Akiror, T. Rahman, and P. Pillay, "Progress on formulas for core loss calculations," *Proc. - 2012 20th Int. Conf. Electr. Mach. ICEM 2012*, pp. 1803–1809, 2012.

[6] P. Roy, M. Towhidi, F. Ahmed, S. Mukundan, and H. Dhulipati, "A Novel Hybrid Technique for Thermal Analysis of Permanent Magnet Synchronous Motor Used in Electric Vehicle Application," *SAE Int.*, pp. 1–9, 2020.

[7] B. Zhang, R. Qu, J. Wang, W. Xu, X. Fan, and Y. Chen, "Thermal Model of Totally Enclosed Water-Cooled Permanent-Magnet Synchronous Machines for Electric Vehicle Application," *IEEE Trans. Ind. Appl.*, vol. 51, no. 4, pp. 3020–3029, 2015.

[8] N. A. Khan, "Power Loss Modeling of Isolated AC / DC Converter," Royal Institute of Technology, 2012.

[9] X. Chen, S. Huang, B. Li, and Y. Xiang, "Losses and thermal calculation scheme of IGBT and FWD and its application in PWM inverters for electric engineering maintenance rolling stock," *IEEJ Trans. Electr. Electron. Eng.*, vol. 13, no. 12, pp. 1822–1828, 2018.

[10] A. Haniff Mahmud, Z. Hilmi Che Daud, and Z. Asus, "the Impact of Battery Operating Temperature and State of Charge on the Lithium-Ion Battery Internal Resistance," *J. Mek.*, vol. 40, no. June, pp. 1–8, 2017.

[11] S. R. Annapragada, M. MacDonald, A. Sur, R. Mahmoudi, and C. Lents, "Hybrid Electric Aircraft Battery Heat Acquisition System," *2018 AIAA/IEEE Electr. Aircr. Technol. Symp. EATS 2018*, pp. 1–13, 2018.

[12] D. Wang, Y. Bao, and J. Shi, "Online lithium-ion battery internal resistance measurement application in state-of-charge estimation using the extended kalman filter," *Energies*, vol. 10, no. 9, 2017.

[13] O. Erdinc, B. Vural, and M. Uzunoglu, "A dynamic lithium-ion battery model considering the effects of temperature and capacity fading," *2009 Int. Conf. Clean Electr. Power, ICCEP 2009*, pp. 383–386, 2009.

[14] S. SDI, "Specification of product INR18650-25R," 2014.

[15] R. Rangappa, S. Rajoo, P. M. Samin, and S. Rajesha, "Compactness analysis of PCM-based cooling systems for lithium battery-operated vehicles," *Int. J. Energy Environ. Eng.*, vol. 11, no. 2, pp. 247–264, 2020.

[16] G. D. Demetriades, H. Z. De La Parra, E. Andersson, and H. Olsson, "A real-time thermal model of a permanent-magnet synchronous motor," *IEEE Trans. Power Electron.*, vol. 25, no. 2, pp. 463–474, 2010.

[17] E. Dlala, M. Solveson, S. Stanton, and A. Arkkio, "Improved model for the preduction of Core Loss in finite element analysis of Electric Machines," in *2015 IEEE International Electric Machines Drives Conference (IEMDC)*, 2015, pp. 340–344.

[18] J. Xu and L. Zhang, "Modeling and Analysis of Temperature Field of Permanent Magnet Synchronous Motor Considering High Frequency Magnetic Field Characteristics," *SAE Int.*, pp. 1–10, 2020.

[19] CERN, "Electrical Power converters Group," *CERN TE Technology Department*, 2020. [Online]. Available: http://epc.web.cern.ch/content/what-power-converter. [Accessed: 15-Apr-2020].

[20] K. Wei, C. Zhang, X. Gong, and T. Kang, "The IGBT Losses Analysis and Calculation of Inverter for Two-seat Electric Aircraft Application," *Energy Procedia*, vol. 105, pp. 2623–2628, 2017.

[21] A. Babaie, B. Karami, and A. Abrishamifar, "Improved equations of switching loss and conduction loss in SPWM multilevel inverters," *7th Power Electron. Drive Syst. Technol. Conf. PEDSTC 2016*, no. Pedstc, pp. 559–564, 2016.

[22] J. Pou, D. Osorno, J. Zaragoza, S. Ceballos, and C. Jaen, "Power Losses Calculation Methodology to Evaluate Inverter Efficiency in Electrical Vehicles," pp. 404–409, 2011.

[23] R. E. Tarter, "Solid-State power Conversion Handbook," Canada: A Wiley-Interscience publication, 1993, pp. 42–63.

[24] M. S. Ali, L. Wang, and G. Chen, "Simulation on SiC based Three Phase Boost Power Factor Correction Rectifier Using MATLAB PLECS Model and its Numerical Analysis Verification," in *The 2nd International Conference on Robotics, Control and Automation Engineering*, 2019, no. 100, pp. 192–197.

[25] MagniX, "Magni500 Specifications," 2020. [Online]. Available: https://magnix.aero/products. [Accessed: 04-Aug-2020].

2021-09-16

Physics-based thermal management system components design for all-electric propulsion systems

Jafari, Soheil

American Society of Mechanical Engineers

Jafari S, Nikolaidis T, Sureddi RC. (2021) Physics-based thermal management system components design for all-electric propulsion systems. In: ASME Turbo Expo 2021: Turbomachinery Technical Conference and Exposition, 7-11 June 2021, Virtual Event, Volume 5B, Paper number GT2021-59995

https://doi.org/10.1115/GT2021-59995